Electrochimica Acta 391 (2021) 138905

Contents lists available at ScienceDirect

Electrochimica Acta

journal homepage: www.elsevier.com/locate/electacta

Mapping experimental and theoretical reactivity descriptors of fe macrocyclic complexes deposited on graphite or on multi walled carbon nanotubes for the oxidation of thiols: Thioglycolic acid oxidation

Ricardo A. Matute[a], Alejandro Toro-Labbé[b], María P. Oyarzún[c], Sara Ramirez[c], Daniela E. Ortega[a], Karina Oyarce[d], Nataly Silva[e,*], José H. Zagal[c,*]

[a] Centro Integrativo de Biología y Química Aplicada (CIBQA), Universidad Bernardo O'Higgins, Santiago 8370854, Chile.
[b] Laboratorio de Química Teórica Computacional (QTC), Facultad de Química y de Farmacia, Pontifica Universidad Católica de Chile, Casilla 306, Correo 22, Santiago, Chile.
[c] Laboratorio de Electrocatálisis, Departamento de Química de los Materiales, Facultad de Química y Biología, Universidad de Santiago de Chile, Av. Libertador Bernardo O'Higgins 3363, Estación Central, Santiago 9170124, Chile.
[d] Universidad Tecnológica Metropolitana, Avenida José Pedro Alessandri 1242, Ñuñoa, Santiago 7800002, Chile.
[e] Facultad de Diseño, Universidad del Desarrollo, Avenida Plaza 680, Las Condes, Santiago 7610658 Chile.

ARTICLE INFO

Article history:
Received 5 February 2021
Revised 3 July 2021
Accepted 6 July 2021
Available online 13 July 2021

Keywords:
Thioglycolic acid oxidation
Metallophthalocyanine
Metalloporphyrin
Volcano correlation
Binding energies
Reactivity descriptors
TOF vs. intermolecular hardness
Multiwalled carbon nanotubes

ABSTRACT

We have studied the electro-oxidation of thioglycolic acid (TGA) catalyzed by iron phthalocyanines and iron porphyrins (FeN4 complexes) deposited on ordinary pyrolytic graphite and on multiwalled carbon nanotubes. The purpose of this work is to establish both experimental and theoretical reactivity descriptors of MN4 macrocyclic complexes for electrooxidation of thioglycolic acid (TGA) as an extension of previous studies involving other reactions using these types of catalysts. Essentially, the reactivity descriptors are all related to the ability of the metal center in the MN4 moiety to coordinate an extra planar ligand that corresponds to the reacting molecule. This coordinating ability, represented by the M-TGA binding energy can be modulated by tuning the electron-donation ability of the ligand and it is linearly correlated with the Fe(III)/(II) redox potential of the complex. Experimental plots of activity as $(\log j)_E$ at constant potential versus the Fe(III)/(II) redox potential of the MN4 catalysts give volcano correlations. A semi-theoretical plot of catalytic activities $(\log j)_E$ vs DFT calculated Fe-TGA binding energies (E_{bTGA}) is consistent with the experimental volcano-type correlations describing both strong and weak binding linear correlations of those volcanos. On the other hand, the Hirshfeld population analysis shows a positive charge on the Fe center of the FeN4 complexes, indicating that electron transfer occurs from the TGA to the Fe center in the FeN4 complexes that act as electron acceptors. The donor (TGA)-acceptor (Fe) intermolecular hardness $\Delta\eta_{DA}$ was also used as reactivity descriptor and the reactivity of the Fe centers as $(\log j)_E$ increase linearly as $\Delta\eta_{DA}$ increases. If activity is considered per active site, the trends is exactly the opposite, i.e. a plot of $(\log TOF)_E$ increases linearly as $\Delta\eta_{DA}$ decreases as expected form the Maximum Hardness-Principle. A plot of $(\log TOF)_E$ versus $E^{o'}_{Fe(III)/(II)}$ gives a linear correlation indicating that the activity per active site increases as the redox potential decreases.

1. Introduction

Macrocyclic MN4 complexes of transition metals, such as metallophthalocyanines (MPcs) and metalloporphyrins (MPs) possess an internal structure involving a central metal coordinated to four pyrrolic nitrogen atoms, similar to molecules found in nature, such as vitamin B_{12}, heme-group in hemoglobin, cytochrome c, chlorophyll, etc [1–4]. MN4 complexes can undergo multiple redox processes centered on the metal involving minimal reorganization energies. As a result, these processes are fast and reversible due to its extended π-electronic system [5,6]. Further, they can act as electron transfer mediators in many reactions, especially when these MN4 molecules are anchored or immobilized on electrode surfaces [6]. A crucial step in these reactions is the coordination of an incoming reacting molecule to the central metal. This involves the

* Corresponding author.
E-mail addresses: nrsilva@udd.cl (N. Silva), jose.zagal@usach.cl (J.H. Zagal).

https://doi.org/10.1016/j.electacta.2021.138905
0013-4686/

formation of a temporary bond between the metal and the reacting molecule and/or intermediates, so the process is essentially inner sphere in nature. In general, the electrocatalytic activity of MPcs and MPs is then controlled by the binding properties of the active site to the incoming molecule [6]. These properties can then be manipulated or controlled by choosing a proper metal or by manipulating the electron-donating properties of the ligand using different substituents. For electrocatalytic reactions, the binding energy of the reacting molecule or intermediates to the active sites on the electrode surface is a well-known reactivity descriptor for metal and alloys but much less studied for molecular catalysts such as MN4 complexes [6]. Previous studies conducted with MN4 complexes have indicated that this is the case for the reduction of molecular oxygen [6–10]. When comparing a wide variety of MN4 complexes having Cr, Mn, Fe and Co as central metals, their electrocatalytic activity, plotted as log of the current density at constant potential $\log(j)_E$ versus the M-O_2 binding energy gives a volcano-shaped curve [6–10]. Starting from low binding energies $\log(i)_E$ increases linearly up to one point and then it decreases for higher binding energies. This follows the Sabatier principle that states that the highest heterogeneous catalytic activity of a process is observed when the "adsorption energy" is not too weak not too strong. Another reactivity descriptor for MN4 catalysts is the M(III)/(II) or/and the M(II)/(I) redox potential, depending on the reaction [3,6–8,11]. This agrees with the fact that, at least for the reduction of O_2 the M-O_2 binding energy and the $E°_{M(III)/(II)}$ for many MN4 catalysts are directly correlated. Further, the metal-centered redox potentials of MN4 complexes correlate linearly with the energy of the frontier orbitals of the complexes. The hardness principle, used as the donor-acceptor intermolecular hardness η_{DA} has also been proposed as a reactivity descriptor for the reduction of O_2 mediated by MN4 complexes, where $\eta_{DA} = \varepsilon_D - \varepsilon_A$, ε_D is the energy of the frontier orbital of the donor MN4 and ε_A is the energy of the frontier orbital of the acceptor (O_2). It was observed that the activity as $(\log j)_E$ increases linearly as η_{DA} decreases for a series of Co phthalocyanines [7,12]. This concept has been followed by Schuhmann and Masa [9,13] for Mn porphyrins and by Mukeerjee [11] for FePcs and observed the same trends in reactivity.

For various reactions studied before [6] it is clear that for a series of complexes with the same metal center, it is possible to modulate their electrocatalytic activity by substituents of different electron-withdrawing character placed on the peripheral and non-peripheral positions of the N4 ligand, which will generate a displacement of the formal potential of the redox pair M(II)/M(I). This displacement of the formal potential can be "tuned" so a hypothetical catalyst would appear at the apex of a volcano correlation. In particular, for the electrocatalytic oxidation of thiols such as l-cysteine [14,15], 2-mercaptoethanol [16], 2-aminoethanethiol [3], glutathione [17,18] and in the oxidation of hydrazine [19,20] for MN4 complexes immobilized on graphite electrodes, volcano correlations have been found. Interestingly, this same trends in reactivity have also been observed using other immobilization strategies of these complexes [21], such as self-assembled monolayers of thiols (SAMs) on gold substrates [22], electropolymerization [23] or covalent and non-covalent incorporation in carbon nanotubes (CNTs) [24–26]. CNTs have been of interest as supporting materials for catalysts because of their special properties as large ratio of surface area to mass, high electrical conductivity and high mechanical strength [27,28]. The properties of the CNTs and MN4 complexes can be coupled generating a synergistic effect. The CNTs increase the intensity of the signals by an area effect, and improve the stability and electrocatalytic activity of the electrode for several reactions of interest, such as, oxidation of thiols [24–26], reduction of oxygen [29,30] and other molecules [31] and it is interesting to examine the reactivity descriptors of MN4 molecules anchored on these carbon nanotubes. Thioglycolic acid (TGA) also known as 2-mercaptoacetic acid ($HSCH_2COOH$), is the simplest and industrially most important mercaptocarboxylic acid [32]. TGA and its derivatives has numerous applications in different areas, highlighting, hair-waving, depilatory products for the cosmetic industry, plastic industries and also in the preparation of culture media [32–34]. Studies on the catalysis of the TGA oxidation reaction have focused mainly on the use of transition metals complexes as oxidizing agents [35–38], although there are few reports on its electrocatalytic oxidation and acid determination using potentiometric techniques [33,34].

In this work, we studied the electrocatalytic activity of a group of iron phthalocyanines (FePcs) and porphyrins (FePs) for the oxidation of TGA. The complexes were adsorbed on two different substrates: directly on pyrolytic graphite (OPG) or on pristine multi-walled carbon nanotubes (MWCNTs) deposited on graphite. Versus its adsorption on pyrolytic graphite (OPG) to obtain a correlation between electrocatalytic activity and the Fe(III)/(II) redox potential.

Density functional theory (DFT) calculations were performed to get more insights about the interaction of substituted iron phthalocyanine and porphyrin catalysts (FePc/FeP) with TGA. DFT calculations were used to estimate the TGA binding energies to the metal in FePc/FeP catalysts and establish how these energies affect the catalytic activity.

2. Methodology

2.1. Materials

Fe(II) 2,9,16,23-tetra(carboxy)phthalocyanine ($4\beta(COO^-)$FePc), Fe(II) 1,2,3,4,8,9,10,11,15,16,17,18,22,23,24,25-hexadecacloro-29*H*,31*H*-phthalocyanine (16(Cl)FePc), Fe(II) 2,9,16,23-tetra(amino) phthalocyanine ($4\beta(NH_2)$FePc), Fe(II) 2,9,16,23-tetra(nitro) phthalocyanine ($4\beta(NO_2)$FePc), Fe(III) 5,10,15,20-(tetra-4-methoxyphenyl) porphyrin chloride (FeTMeOP), Fe(III) 5,10,15,20-(tetra-4-pyridyl) porphyrin chloride (4(4-py)FeP) and iron(III) 5,10,15,20-(tetraphenyl)porphyrin chloride (4(ph)FeP) were obtained from PorphyChem (Dijon,France). The Fe(III) 4,4,4,4-tetrasulfonic acid phthalocyanine ($4\beta(SO_3^-)$FePc) and Fe(II) phthalocyanine (FePc) were obtained from Sigma Aldrich. All the metal complexes were used as provided.

Pristine multi-walled carbon nanotubes (MWCNT-p) were acquired from Dropsens (diameter 10 nm, and length of 1-2 μm). MWCNT-p were purified in 37% HCl solution for 5 days and then refluxed for 5 h, followed by thoroughly washing with water and acetone. N,N-dimethylformamide (DMF) (analytical grade). HCl, acetone, NaOH and thioglycolic acid (≥99.0%) were provided by Merck. The solutions were prepared with Milli Q water (Millipore, Inc.).

2.2. Preparation of hybrid materials between MWCNTs and Fe complexes

The hybrid materials containing iron phthalocyanine and porphyrin complexes (FeC) and MWCNT-p were obtained using methodologies previously reported [26]. MWCNT-p were dispersed in phthalocyanine solutions (1 mg mL^{-1}) by sonication for 30 min. The suspensions were left to rest for 24 hours at room temperature and were then filtered and washed with the corresponding solvent and ethanol to remove any excess of the complexes. This procedure was to avoid the formation of complex microcrystals where the molecules are not directly attached to the CNT walls. The solid was dried in oven at 40 °C for 24 h. Finally, MWCNT/FeN4 suspensions in DMF (1 mg mL^{-1}) were prepared.

2.3. Preparation of modified electrodes

Before each experiment, the surface of the OPG electrode was mechanically polished with 2400 grit emery paper followed by ultrasonic treatment in purified water for 2 min and dried under a nitrogen flow. Electrodes were modified placing a drop (10 μL) of the 1 10^{-4} M complex solution or 1 mg mL^{-1} of the hybrid materials. Then, the electrodes were thoroughly washed with DMF to eliminate any excess of the complex or hybrid materials. All the complex solutions were prepared using DMF, except for 4β(COO^-)FePc and 4β(SO_3^-)FePc which were dissolved in water.

2.4. Electrochemical measurements

Cyclic (CV) and linear sweep (LSV) voltammetry experiments were carried with a BAS i-Epsilon electrochemical workstation using a conventional three-electrode glass cell. A basal-plane pyrolytic graphite electrode (OPG), from Pine Research was used as the working electrode. A platinum spiral wire of 5 cm^2 geometric area and an Ag/AgCl 3M electrode were used as the auxiliary and reference electrodes respectively. Measurements were carried out at 25 °C in a 0.1 M NaOH N_2-saturated solution (pH 13). Cyclic voltammetry was used to determine the formal potential and the surface concentration of the different Fe complexes. CV curves were obtained under N_2 saturated solutions. Scan rate 0.1 V s^{-1}. The surface concentration (Γ) of Fe complexes and different hybrid MWCTs/Fe complexes on the electrode was estimated from the electrical charge (Q) estimated from the integration of the area under the CV peaks of the redox peaks of the Fe(III)/(II) redox process using the following equation: $\Gamma = \frac{Q}{nFA}$ where, n is the number transferred electrons and for this case equal to one, F Faraday constant and A is the geometric electrode area (0.196 cm^2). Polarization curves were obtained in N_2 saturated 5 mM TGA solutions using a scan rate 0.005 V s^{-1} and rotation speed of 800 rpm.

2.5. Computational details

Density Functional Theory (DFT) calculations were performed to investigate the binding energies of substituted iron phthalocyanines and porphyrins (FePc/FeP) to thioglycolic acid (TGA). The geometry of the systems was optimized using ORCA 4.0 program [39] with the unrestricted formalism for all open shell systems. Perdew–Burke–Ernzerhof (PBE) functional [40] was used with the relativistic effective core potential Stuttgart Dresden basis set (SDD) [41] for the Fe atom and the all-electron Ahlrichs polarized double zeta basis sets (SVP) [42] for H, C, N, O, S and Cl atoms for the substituted Fe-phthalocyanines/porphyrins and TGA structures. This methodology has been reported to provide adequate results for the O_2 reduction mediated by FeN4s [43] in good agreement with more costly DFT methods. The DFT-D3 [44] dispersion corrections were used in order to include dispersion force effects on energy. Counterpoise corrections were also made for basis set superposition error (BSSE) [45]. All structures were optimized in a water solution described by the conductor-like polarizable continuum model (CPCM) [46].

The TGA binding energies (E_{bTGA}) for the substituted FeN4 were evaluated using the following equation:

$$E_{bTGA} = E_{FeN4-TGA} - (E_{FeN4} + E_{TGA})$$

Where E_{FeN4} and E_{TGA} are the energies of the isolated optimized structures of the substituted FePc and FeP complexes and the TGA molecule, respectively, and $E_{FeN4-TGA}$ is the energy of the optimized structure of the TGA adduct. Therefore, negative values indicate that TGA molecule would be energetically favorable to be coordinated (oxidized) by FeN_4, while positive values indicate that TGA molecule is not able to oxidize the FeN4.

For the reactivity study, the electronic distribution on the complexes was analyzed by Hirshfeld atomic charges [47] using the Multiwfn [45] analyzer. The binding nature of the FeN4 have been analyzed using the atoms in molecules (AIM) [48] method. The charge on the metal center before and after binding with TGA as well as the net charge on TGA molecule in the adduct structure was computed. Additionally, the electron density difference [$\Delta\rho$(r)] was obtained to get insights into the electron density distribution after the TGA binding adduct. This property was computed as:

$$\Delta\rho(r) = \rho_{FeN4-TGA}(r) - \rho_{FeN4}(r) - \rho_{TGA}(r)$$

Where $\rho_{FeN4-TGA}(r)$ is the electron density of TGA adduct, while $\rho_{FeC}(r)$ and $\rho_{TGA}(r)$ are the electron densities of the separate FeN4 and TGA molecule, respectively.

3. Results and discussion

The schematic structures of the iron phthalocyanine and iron porphyrin complexes and of thioglycolic acid are illustrated in Fig. 1. The complexes have different peripheral and non-peripheral substituents compared to the unsubstituted FePc, with either electron-donating or electron-withdrawing groups which affect directly the electron density of the metallic center. Therefore, when using complexes with the same metal center, Fe in this case, it is possible to modulate the electrocatalytic activity to obtain the maximum activity according to the substituent [6-10,12,14–19].

Fig. 2 shows cyclic voltammograms of FePc on OPG electrode measured in N_2-saturated 0.1 M NaOH solution. All Fe phthalocyanine CV curves shows two characteristic and reversible redox processes centered on the metal center [26]. The first peak at more negative potentials has been attributed to the Fe(II)/(I) redox couple and the second peak to the Fe(III)/(II) redox couple [26]. The porphyrins show CV curves that are shifted towards more negative potentials as a result of the more electron-donating character of the porphyrin ligand compared to the phthalocyanine. The Fe(II)/(I) redox pair does not appear under the working conditions. For some reason, the 4(4-py)FeP complex shows very irreversible redox peaks which is barely visible in Fig. 2. A more expanded version of that is shown in Fig. S1 shows an anodic peak at -0.664 V and a cathodic peak at -0.946V giving an average value for this process of -0.805 V. Values for all complexes are listed in Table 1.

The cyclic voltammograms of the MWCNT/FePc hybrids in Fig. 3 show similar behavior compared to the data in Fig. 2, with a considerable increase in the currents with respect to FePc adsorbed on OPG, mainly due to the increase in the electrode surface area. The presence of MWCNT does not affect the redox processes of the FePc complex in a visible way. Table 1 shows the mean values of redox potentials of the series of FePc complexes and MWCNT/FePc hybrid materials adsorbed on the OPG electrode. MWCNT/4(4-py)FeP complex shows more pronounced peaks compared to those observed in the absence of MWCNT anodic (-0.652V) and cathodic (-0.960V) irreversible peaks centered around. -0.806V. An amplified version of those peaks is shown in Fig. S1.

In Fig. 4 we compare the polarization curves obtained on several FePc/OPG and FePc/MWCNT/OPG hybrid materials for the oxidation of TGA. The response of the OPG and MWCNT/OPG electrodes without FePc complexes is also shown. All systems show a response except for those systems without Fe complexes. None of the polarization curves reach a mass transport limiting current, because the Fe(III)/(II) formal potential is close to that of the maximum current reached in the polarization curve. The maximum current is then a chemically limited current as the fraction of Fe(II) starts to decrease as the potential becomes more positive. The decrease in the currents at more positive potentials more or less coincides with the oxidation of Fe(II) centers to Fe(III). The Fe (III)

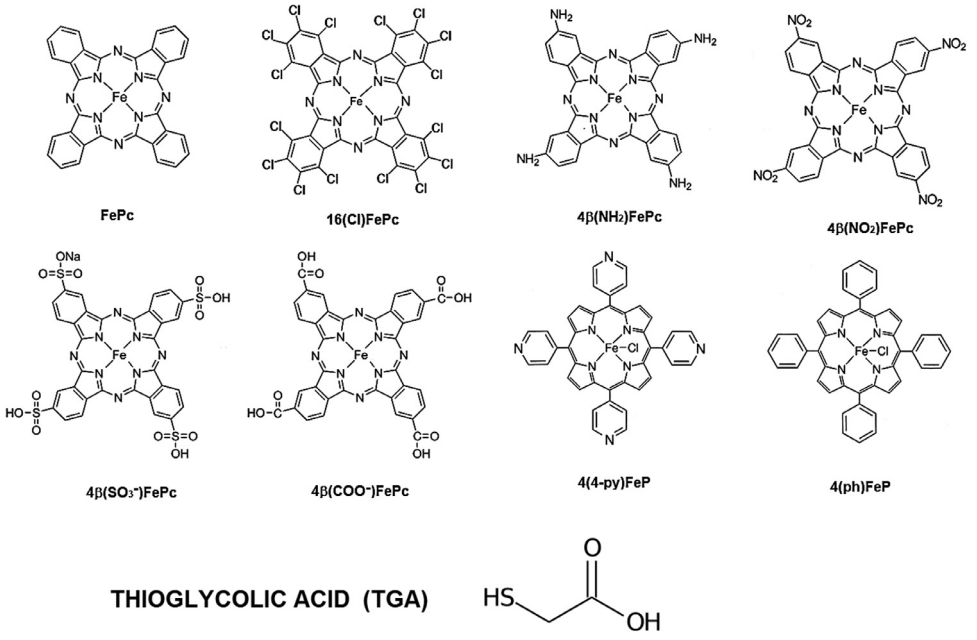

Fig. 1. Structures of the studied Fe complexes (phthalocyanines and porphyrins) bearing different substituents and of thioglycolic acid.

Table 1
Electrochemical parameters. $E^{\circ\prime}$ formal potentials, charges (Q) and surface coverage (Γ) from cyclic voltammograms (0.1M NaOH N_2-saturated solution. Scan rate: 0.1 V s^{-1}), onset from polarization curves of the electro-oxidation of 5 mM TGA; Tafel slope 5 mM TGA in 0.1 M NaOH N_2-saturated solution.

	OPG/MN4					OPG/MWCNT/MN4				
MN4	$E^{\circ\prime}$(III/II)/V	Q/C cm^{-2}	Γ/mol cm^{-2}	Onset	b/V_{dec-1}	$E^{\circ\prime}$ (III/II)/V	Q/C cm^{-2}	Γ/mol cm^{-2}	Onset	b/V_{dec-1}
FePc	-0.129	4,888E-05	5,066E-10	-0.443	0.078	-0.133	1,582E-04	1,640E-09	-0.326	0.073
4β(NH_2)FePc	-0.187	8,348E-05	8,652E-10	-0.399	0.075	-0.184	3,720E-05	3,856E-10	-0.355	0.066
4β(SO_3^-)FePc	-0.081	4,578E-05	4,745E-10	-0.403	0.089	-0.082	1,695E-04	1,757E-09	-0.371	0.075
4β(COO^-)FePc	-0.089	7,681E-05	7,961E-10	-0.458	0.084	-0.102	1,047E-04	1,085E-09	-0.317	0.079
4β(NO_2)FePc	-0.215	1,199E-04	1,243E-09	-0.446	0.074	-0.187	1,703E-04	1,765E-09	-0.364	0.063
16(Cl)FePc	-0.016	7,512E-05	7,786E-10	-0.396	0.119	-0.042	8,989E-05	9,317E-10	-0.363	0.069
4(4-py)FeP	-0.805	9,623E-05	9,974E-10	-0.110	0.289	-0.806	6,741E-04	6,987E-09	-0.356	0.155
4(ph)FeP	-0.590	5,517E-05	5,718E-10	-0.016	0.258	-0.635	7,235E-04	7,499E-09	-0.321	0.172

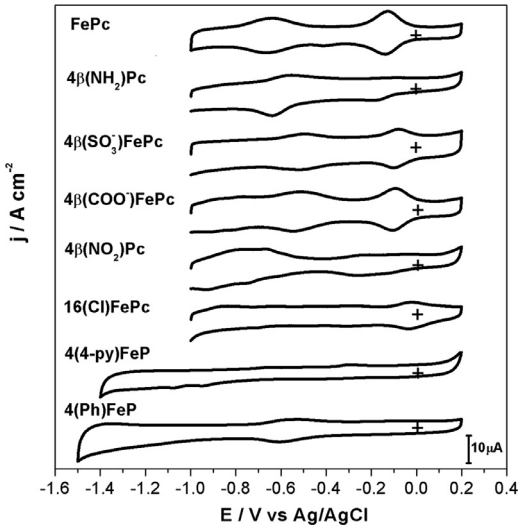

Fig. 2. Cyclic voltammograms of OPG electrode modified with (a) FePcs and FePs complexes. N_2-saturated 0.1 M NaOH solution. Scan rate: 0.1 V s^{-1}.

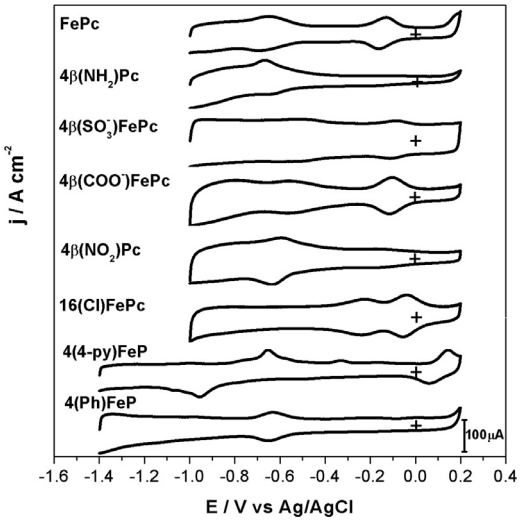

Fig. 3. Cyclic voltammograms of OPG electrode modified with MWCNT/FePcs and MWCNT/FePs. N_2-saturated 0.1M NaOH solution. Scan rate: 0.1 V s^{-1}.

state has no catalytic activity because the sites are blocked by OH^- strongly coordinated to the Fe (III) centers [24–26]. Fe porphyrins exhibit very low activity as they are predominantly in the inactive state Fe(III)OH. They only exhibit a foot of a wave that occurs at potentials close to the oxygen evolution reaction (OER).. Since porphyrins exhibit poor catalytic activity for the oxidation of TGA and require high overpotentials it is possible that oxygen evolution occurs in the potential range 0.4- 0.6 V [49]. In order

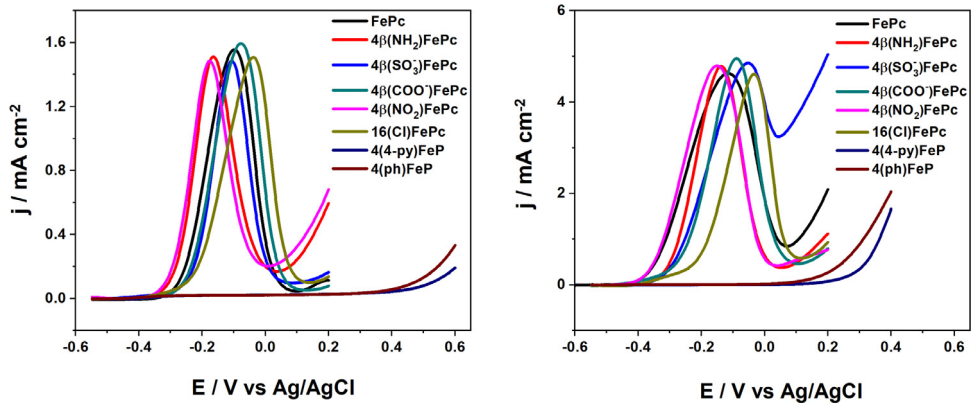

Fig. 4. Polarization curves obtained from oxidation of TGA 5 mM in NaOH 0.1 M on OPG electrode modified with (a) FePcs and FePs complexes; and (b) MWCNT/FePcs and MWCNT/FePs. N_2-saturated solution; Scan rate: 0.005 V s^{-1}, rotation rate: 1600 rpm.

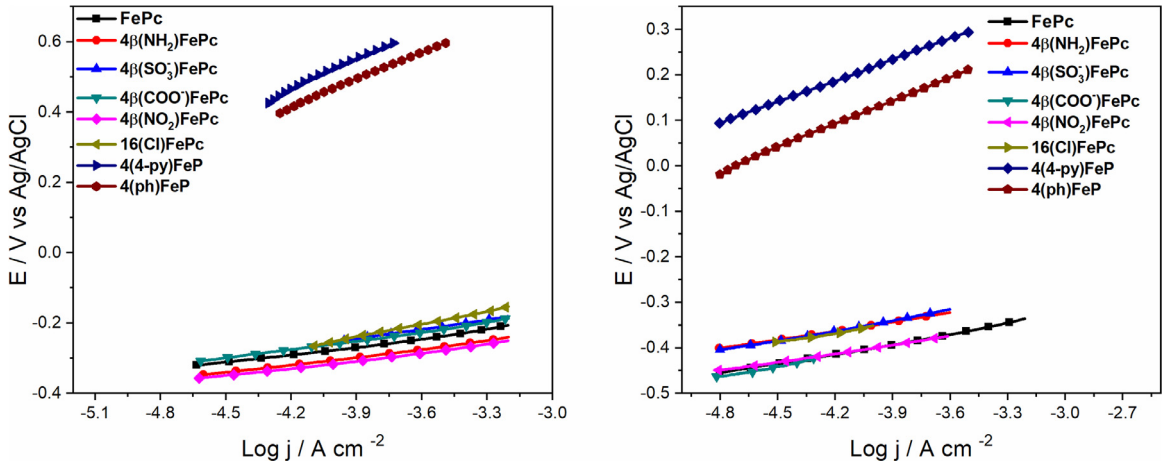

Fig. 5. Tafel slopes obtained from polarization curves for oxidation of TGA 5 mM in NaOH 0.1 M on OPG electrodes modified with (a) FePcs and FePs complexes and (b) MWCNT/FePcs and MWCNT/FePs.

to check if dithioglycolic acid is indeed formed at potentials beyond the foot of the wave of TGA oxidation in Fig. 4 a series of controlled-potential electrolysis experiments were conducted with 0.005 M TGA solutions in 0.1 M NaOH, using the same working electrode employed for all experiments i.e.: (MWCNT/4(4py)FeP) in order to have exactly the same working conditions. We did not test 4(ph)FeP which is more active. The potential was set at 0.45 V, details are given in the Supporting Information. The electrode was found to lose some activity over the time involved in the experiment (ca. 20 h) with a loss of activity of ca. 30-40% over the period of the electrolysis. Both unreacted TGA and dithiodiglycolic acid (DTDGA) were separated using analytical paper chromatography (phenol + water as eluent) and compared with authentic samples of TGA and DTDGA. UPLC chromatogratography was also used to detect the presence of DTDGA. This product was found to be the main product of the reaction (see Fig. S7) but the formation of O_2 via a parallel route cannot be discarded, especially for 4(ph)FeP which was not tested for product formation but since it more active, probably forms less O_2 than 4(4py)FeP.

Fig. 5 shows Tafel plots obtained from the low overpotential kinetic-controlled current region of Fig. 4. Two linear regions are observed, one corresponding to the FePcs with values of ~ 0.060 V dec^{-1} and the other for the FePs, with values > 0.20 V dec^{-1} (Table 1), suggesting that there are two different ET mechanisms for TGA electro-oxidation. The low catalytic activity of FePcs can be attributed to the fact that these complexes have a very negative Fe(III)/(II) redox pair. Therefore, at the potential where oxidation currents are observed, most of the molecules are in the inactive Fe $[(III)OH^-]_{ad}$ state so the Fe(II) surface concentration is rather low. The high Tafel slopes, well above 0.12 V dec^{-1} are observed for Fe porphyrins where the surface is covered mostly with Fe(III)OH species. It is possible that the strongly adsorbed OH^- ion induce some inhibition of the process. This has also been observed for the oxidation of formic acid on Pd where adsorbed phosphate anion inhibits the process and the Tafel slopes are as high as 0.500 V dec^{-1} [50]. It is interesting to note that these high slopes are also observed for FePcs for the second oxidation wave after the first wave for TGA oxidation. At the potentials of the second wave the FePcs are predominantly as Fe(III)OH, see Fig. S4 and Table S4 so they behave like Fe porphyrins.

Fig. 6 shows plots of (log $j)_E$ at a constant potential (-0.3 V) versus the formal potential of the Fe(III)/(II) redox couple of each catalyst. Both correlations have the typical volcano shape that correlates the activity of the metal essentially with the ability of the central metal to donate or accept electrons [6,11,18–21,26,27]. One of the legs of the volcano includes only FePcs and the other only FePs. This illustrates that it is possible to "tune" the formal potential of the catalyst, manipulating its chemical structure to obtain maximum electrocatalytic activity for the reaction under study and indeed for many other reactions [2,6–8,11,12,16,18,19,22,25,26,29,33,51]. In this case this is observed when working at a potential of -0.3 V and it is expected that the complexes with the highest activity are those that at that particular potential the Fe (II) active species adsorbed on the surface pre-

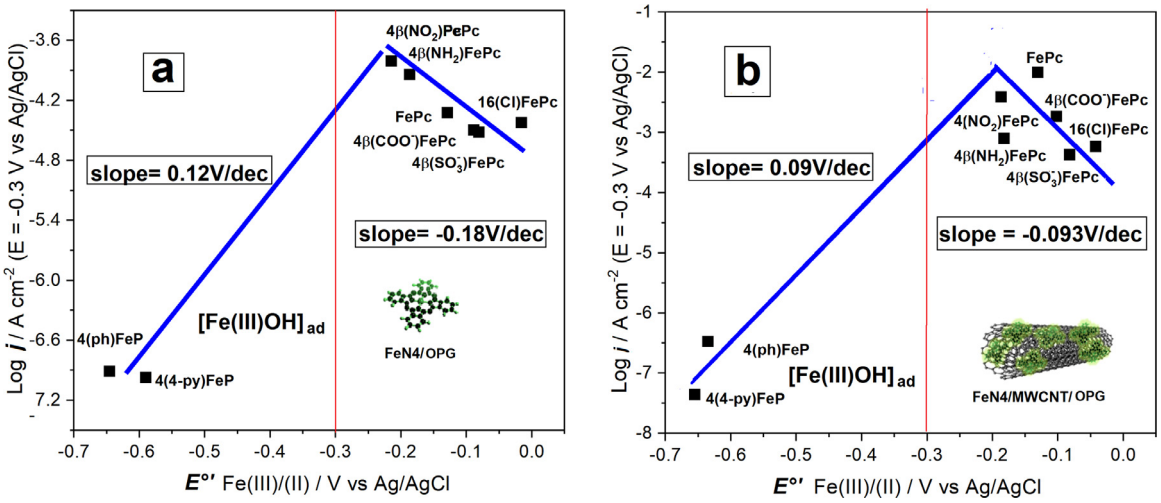

Fig. 6. Log *j* (E =-0.3 V) versus the formal potential *E*°Fe(III)/(II) of the catalyst for the electro-oxidation of TGA using OPG electrodes modified with (a) FePcs and FePs complexes; (b) with MWCNT/FePcs and MWCNT/FePs.

dominate, which is the case for the FePcs. The potential of -0.3 V was chosen as to avoid too much extrapolation of the currents observed for the more active catalysts. FePs present Fe(III)/(II) redox potentials that are well below -0.3 V and the surface concentration of Fe(II) active sites is very small at that particular potential. The red line indicates the potential of the electrode to emphasize that complexes located to the left of the red lines are predominantly as Fe(III)OH. We have discussed in detail this issue for cysteamine oxidation reaction [25] catalyzed by the same complexes and the response correlates with a semi-quantitative modeling of the experimental observations.

The slope of the left-hand side of the volcano in Fig. 6(a), that groups the Fe porphyrins is +0.134 V dec^{-1} whereas the line that groups the Fe phthalocyanines is -0.223 V dec^{-1}. For the data involving MWCNTs/ FeN4 (Fig. 6(b)) the corresponding slopes are +0.103 V dec^{-1} and -0.069 V dec^{-1}. It is important to point out that two or three data points on one side of the volcano is insufficient to draw a straight line and estimate a slope. It is also possible that those currents are contaminated with contributions from the oxygen evolution reaction that takes place at the high positive potentials where TGA oxidation was tested. The value of the slope is then a rough estimation, or better, shows a trend. Further, to draw a line on the left side of the volcano we are assuming that the volcano correlation is almost symmetrical. We will discuss further down the theoretical interpretation of these slopes, but we can state that the values of the slopes are close to +/- 0.118 V dec^{-1} or 2.303x$RT/\beta F$ (β~ 0.5) at T=25°C are rough estimations, especially for the FePcs.

The data in Fig. 6 clearly indicates that the $E^{\circ\prime}$ $M^{+/(n-1)+}$ formal potential of the catalyst is a reactivity descriptor for this particular reaction as observed for many reactions [3,6,7,9,13–20,23–25,30]. Recently, attention has been focused on two reactivity descriptors, the active metal site density (*SD* [mol_{site} cm^{-2}], and the catalytic turn-over frequency (*TOF* [s^{-1}] or [*electron site*$^{-1}$ s^{-1}]), that is the electrons transferred per active site per second [52]. Increasing the value of one, or both of these descriptors, in fact leads to the synthesis of intrinsically highly active electrocatalysts. A rather simple way of comparing the catalytic activity of different catalysts with data like the one illustrated in Fig. 7 is simply as: $TOF = j/(Q_{\text{effect}})$ in electron s^{-1} at a given potential, where j is the current density in A cm^{-2} (or C cm^{-2} s^{-1}) and Q is the effective electrical charge in C cm^{-2}. Q can be obtained from the average charge under each redox peak. Q_{effect} is the effective electrical charge that can be attributed only to Fe(II) active sites available for the reaction at

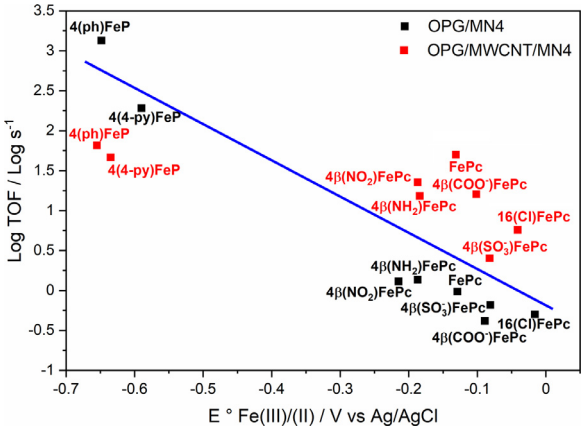

Fig. 7. Log *TOF* versus formal potential *E*° Fe(III)/Fe(II) of the catalyst for the electro-oxidation of TGA using OPG electrodes modified with (a) FePcs y FePs complexes; (b) with MWCNT/FePcs and MWCNT/FePs.

a given potential, no bulk FeN4 complexes or Fe(III) sites. In our case we have little or no bulk catalysts as the FeN4 complexes are nearly monolayers since the modified electrodes were thoroughly rinsed with the solvent to remove any excess of complex from the surface. Another consideration is $Q_{\text{effec}} = \theta_{\text{Fe(II)}}Q$. The fraction of surface concentration of Fe sites in the Fe(II) active state $\theta_{\text{Fe(II)}}$ at a given potential can be calculated using the Nernst equation for adsorbed species exhibiting an EE processes [8,25,53] and assuming ideal behavior. Since the catalytic currents are observed at potentials much more positive than $E^{\circ}_{II/I}$, *i.e.* $E >> E^{\circ}_{II/I}$ the first term is practically unity. It is important to point out again that if the currents measured with Fe porphyrins are contaminated with OER currents the *TOFs* for Fe porphyrins should be lower since the true currents for TGA oxidation are less than those used for calculating the *TOF* values.

$$\theta Fe(II) = \frac{\exp\left(F\left(E - E^{0}_{II/I}\right)/RT\right)}{\left[1+\exp\left(F\left(E - E^{0}_{II/I}\right)/RT\right)\right]}\frac{1}{\left[1+\exp\left(F\left(E - E^{0}_{III/II}\right)/RT\right)\right]} \quad (1.1)$$

So for $E >> E^{\circ}_{II/I}$

$$\theta Fe(II) \sim \frac{1}{\left[1+\exp\left(F\left(E - E^{0}_{III/II}\right)/RT\right)\right]} \quad (1.2)$$

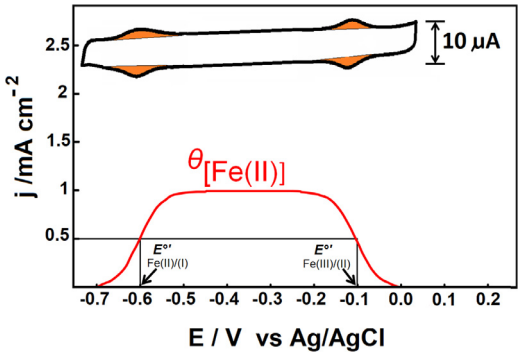

Fig. 8. Hypothetical potential dependence of the surface coverage $\theta_{Fe(II)}$ using the Nernst equation as eq.(1) (red line) assuming $E°'$ Fe(II)/(I) = - 0.6 V and $E°'$ Fe(III)/(II) = -0.1 V and illustrated with a cyclic voltammogram profile.

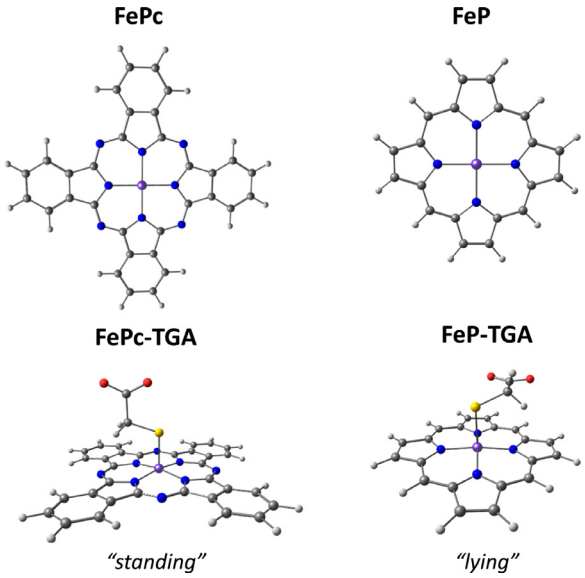

Fig. 9. FePc-TGA and FeP-TGA systems: "standing" TGA on phthalocyanine and "lying" TGA conformation on porphyrin.

This expression carries the assumption that the adsorbed species behave ideally and this is possible since the Fe centers on the adsorbed or anchored FeN4 complexes will be separated by distances comparable to the diameter of the porphyrin or phthalocyanine molecule.

Fig. 8 illustrates how $\theta_{Fe(II)}$ varies with potential according to equation (1) and the hypothetical oxidation current for TGA. The curve describing $\theta_{Fe(II)}$ reaches the value 0.5 at $E = E°'$Fe(II)/(I) and $E = E°'$Fe(III)/(II) so any catalyst should be active in the potential window where Fe(II) predominates. It is clear from Fig. 8 that the activity should decrease if the potential of the electrode becomes more positive than $E°'$Fe(III)/(II) as the Fe center evolves to the inactive Fe(III)OH as observed experimentally in Fig. 4. This indicates a de-activation/inhibition step as discussed by Limoges and Savèant for the reversible deactivation of enzymes [54].

Fig. 7 clearly demonstrates that the reactivity per active site (as *TOF*) increases as the Fe(III)/(II) formal potential decreases and provides a linear correlation of slope -0.25 V dec^{-1} and resembles one linear region of the volcano correlation that groups the FePcs in Fig. 6. From the practical point of view for this particular reaction the high *TOF* values do not imply high catalytic activity since the surface density of active Fe(II) sites (*SD* $[mol_{site}\ cm^{-2}]$ is very low for those catalysts exhibiting high *TOF* values, so the total, experimental activity as a current density is low, as shown in the volcano correlation of Fig. 6. It is surprising however that the reactivity per active site increases when the redox potential becomes more negative. One would expect that the most oxidizing complexes, i.e. those with more positive Fe(III)/(II) formal potentials would be more active as the formal potential contribute to the driving force of the reaction. This is in contrast to the reactivity trends observed for ORR on MN4 catalysts where the reactivity per active site increases as the driving force of the catalysts increases, that is, activity increases as $E°'$M(III)/(II) becomes for negative [8].

To better understand the role of the substituents on iron phthalocyanine and porphyrin complexes and their effect on the catalytic activities for TGA electro-oxidation, we performed DFT calculations analyzing their electronic properties. We found two stable conformations for the TGA binding on the substituted FePc and FeP complexes; "standing" and "lying" TGA on phthalocyanine and porphyrin catalyst, respectively as illustrated in Fig. 9.

For the "standing" conformation, the TGA molecule presents the –COO$^-$ group of the TGA structure away from the phthalocyanine surface and the S atom is placed on top of Fe atom at 2.16 A. While, the "lying" conformation shows the TGA molecule with the –COO$^-$ group directed toward the porphyrin surface, and the S atom is placed at 2.35 A of the Fe atom. Both conformations, also were found as the most stable conformations for the substituted FePc complexes, while for FeP complexes, the "lying" conformation was preferred (Fig. 10).

TGA binding energies (E_{bTGA}) for the substituted FeC, the charges of the metal center (Fe) before (complex) and after (adduct) binding with TGA and the Fe-S distances for each catalyst are listed in Table 2. Firstly, the interaction of the TGA molecule for the "standing" and "lying" conformations are binding onto catalysts at distances of ~2.16 and ~2.36 A on average in all the cases for "standing" and "lying" conformations. The latter indicates that the "standing" conformation is favored, suggesting that there is no interaction of the catalyst surface with the COO$^-$ group of the TGA molecule, a spatial arrangement that seems to allow a greater stabilization of the adduct. However, according to results given by binding energies, for both conformations all values are negative, which means that the binding (oxidation) is favorable. In addition, the most negative binding energies belongs to the phthalocyanine family specifically to the "standing" conformation, hence this conformation has been identified as the most energetically stable geometry. It should also be noted that the electron-withdrawing substituents presents the most negative binding energies resulted in increased of the experimental catalytic activities as shown the volcano correlation in Fig. 11, which appears in the strong binding side (left). On the weak binding side (right) appears the phthalocyanine functionalized by NH_2 group (electron-donating) and the functionalized porphyrins, consistently displayed lower catalytic activities. These results clearly indicate that the introduction of electron-withdrawing substituents on FePc facilitates the oxidation process.

Since comparing electrocatalytic activities of the different FeN4 catalysts using two reactivity descriptors namely the $E°'$ Fe(III)/(II) formal potentials and the Fe-TGA binding energies both exhibit volcano correlations (Figs. 6 and 11) it is interesting then to compare the formal potentials $E°'$ Fe(III)/(II) formal potentials versus the FeN4-TGA binding energies. This is illustrated in Fig. S5 and in spite of the dispersion of the data, there is a clear trend where higher binding energies (more negative) mean more positive redox potentials. It has been shown in previous work for the reduction of O_2 on a great variety of MN4 catalysts involving Cr, Mn, Fe and Co as metal centers that the correlation between M-O_2 binding energies and $E°'$ M(III)/(II) formal potentials is essentially linear [8]. Our results and those reported previously [8] indicate that these two

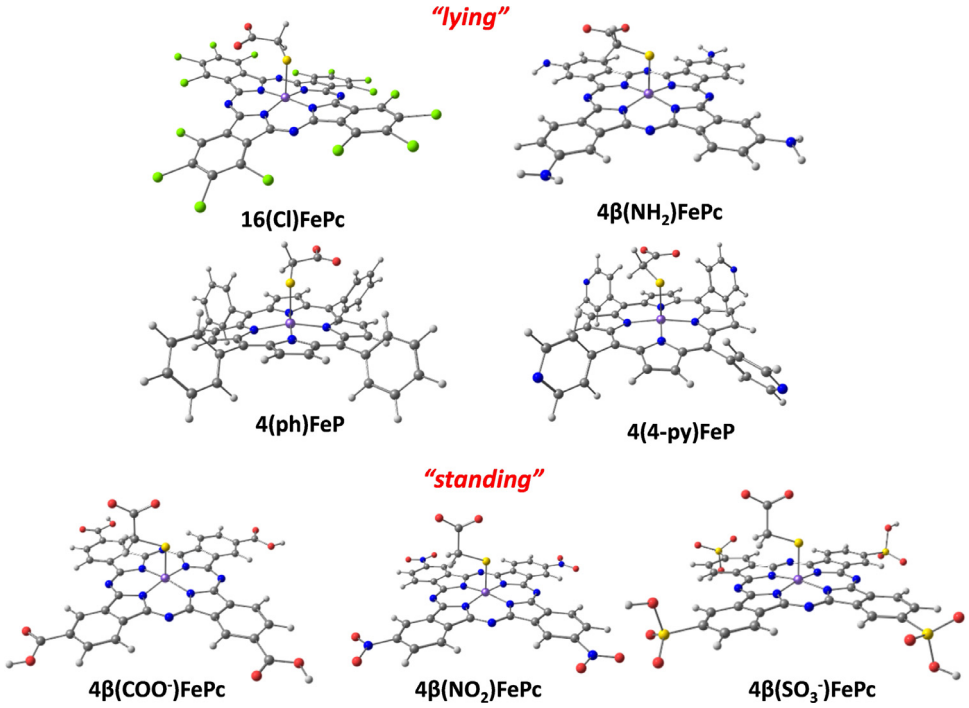

Fig. 10. "standing" and "lying" TGA conformations on substituted FePc and FeP complexes.

Table 2
TGA binding energies, charges of the metal center (Fe) before (complex) and after (adduct) binding with TGA and the Fe-S distances for each catalyst.

System	E_{bTGA} (eV)	$Q_{Fe(complex)}$ (|e|)	$Q_{Fe(adduct)}$ (|e|)	$d_{Fe\text{-}S(adduct)}$ (A)
Phthalocyanines				
FePc	-2.174	0.178	0.297	2.16
16(Cl)FePc	-2.473	0.210	0.154	2.35
$4\beta(COO^{-})$FePc	-2.338	0.177	0.162	2.16
$4\beta(NH_2)$FePc	-1.706	0.102	0.118	2.36
$4\beta(NO_2)$FePc	-2.704	0.179	0.215	2.17
$4\beta(SO_3^{-})$FePc	-2.506	0.181	0.126	2.16
Porphyrins				
4(ph)FeP	-1.738	0.136	0.188	2.34
4(4-py)Fep	-1.988	0.147	0.196	2.35

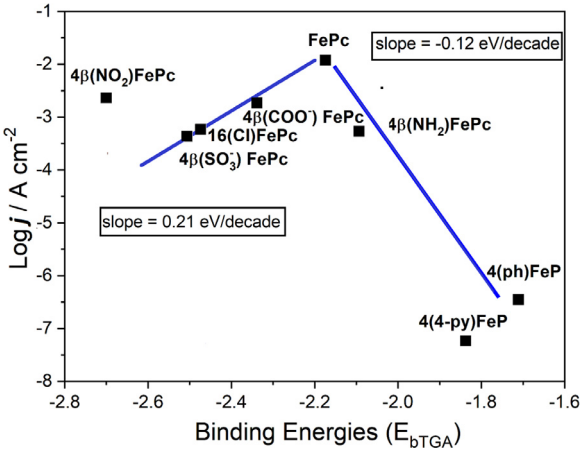

Fig. 11. Volcano correlation for TGA oxidation. Catalytic activities (Log *j*) OPG/FeN4 on axis Y vs DFT TGA binding energies (E_{bTGA})/eV on axis X for Fe-phthalocyanines and porphyrins catalysts.

reactivity descriptors are directly correlated and it is likely that this is true for many reactions.

On the other hand, Hirshfeld population analysis shows the positive charge on Fe center in the complex is smaller than that in the adduct (see Table 2), which indicates electron transfer density from the TGA molecule to the phthalocyanine and porphyrin complex. These results support the point of view that the catalysts act as an electron acceptor. In this context, the highest occupied molecular orbital (HOMO) and lowest unoccupied molecular orbital (LUMO) are associated to both TGA and FePc/FeP molecules and can be combined to form the orbitals of the adducts. The donor–acceptor hardness [55] (supporting information, Table S2) was calculated in order to quantify the affinity between the donor (TGA) and the acceptor (FePc/FeP catalysts) species. Small values of $\Delta\eta_{DA}$ indicate a small energy gap.

It can be noted that the adducts with "standing" conformation (FePc, 4β-(COO^{-})FePc, 4β-(NO_2)FePc and 4β-(SO_3)FePc) have the higher $\Delta\eta_{DA}$ values and higher catalytic activities and binding energies toward TGA. Also note that $\Delta\eta_{DA}$ values are higher for the phthalocyanines family than porphyrins. Besides, the electron-withdrawing substituents on FePc induce smaller values of $\Delta\eta_{DA}$ in agreement with the volcano correlation (Fig. 11). This was confirmed by plotting the electron density difference (see Fig. S3). associated to the adducts. In this regard, electron density difference reveals the charge density distributions in the adduct systems by

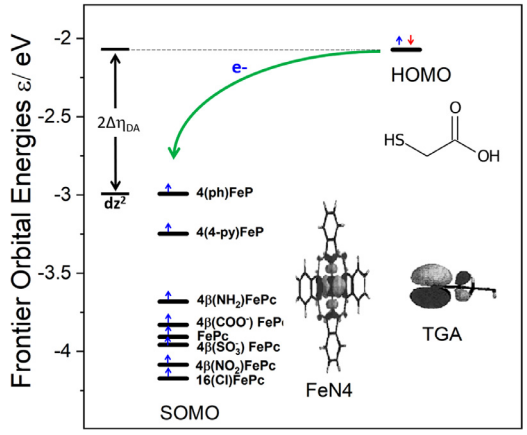

Fig. 12. Diagram of the energy gaps (donor-acceptor intermolecular hardness $2\Delta\eta_{DA}$) of the frontier orbitals of TGA (HOMO) and of the different FeN4 complexes (SOMO). Molecular orbital profiles taken from [7].

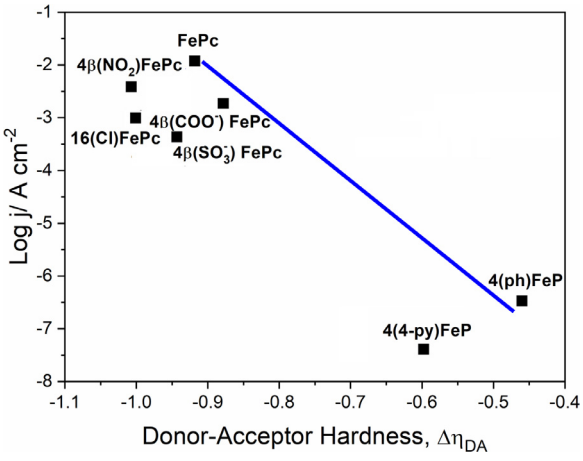

Fig. 13. Correlation between catalytic activity as $(\log j)_E$ versus the donor-acceptor intermolecular hardness for TGA oxidation activated by FeN4 complexes.

means of the negative (sky blue color) and positive (yellow color) charge excesses. In the TGA molecule and the Fe atom the negative charge is localized, while the positive charge is mainly located in the ligands. Therefore, the TGA binding activates the Fe atom, both electrostatically interact with the electron deficient atoms of the ligands, increasing the adducts stabilities depending of the nature of the functionalized group for the phthalocyanine and porphyrin families. Q_{Fe} charges in the adduct for the phthalocyanine family appear to be of the order of FePc > $4\beta(NO_2)$FePc > $4\beta(COO^-)$FePc > 16(Cl)FePc > $4\beta(SO_3)$FePc > $4\beta(NH_2)$FePc (see Table 2), which is strongly correlated with the volcano. This again suggests that the nature of the electron-donating and electron-withdrawing groups plays a very important role in terms of electrostatic interactions on the catalytic activity of the phthalocyanine. Presumably, electron-withdrawing groups remotely activate the metallic center, decreasing the electron density on the Fe atom, which improve the oxidization of the Fe and increases the catalytic activity.

Fig. 12 shows a diagram of the energies frontier orbitals of the donor (TGA) and the acceptor (FeN4 complexes). The hardness $\Delta\eta_{DA}$ is one half the energy gap between the orbitals of the donor and of the acceptor. According to the principle of minimum hardness, the highest reactivity should be observed for the FeN4 complex having the highest SOMO nergy and closer to the HOMO of TGA, i.e. for 4(ph)FeP. Fig. 13 compares the activity as $(\log j)_E$ versus $\Delta\eta_{DA}$ for the whole series of FeN4 complexes and the trend in reactivity is the opposite to that predicted by the minimum molec-

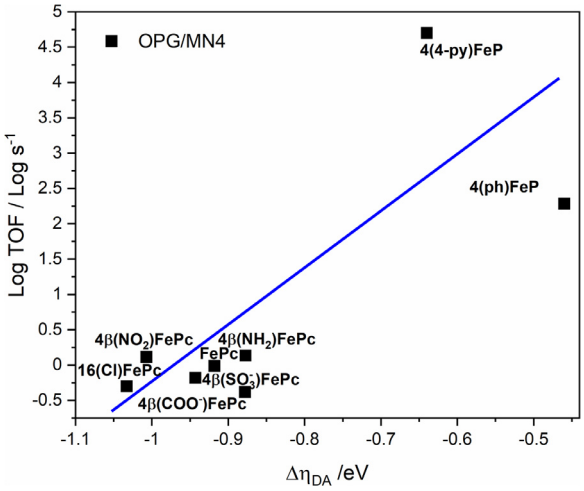

Fig. 14. Correlation between catalytic activity as $(\log TOF)_E$ versus the donor-acceptor intermolecular hardness for TGA oxidation activated by FeN4 complexes.

ular hardness principle. For example 4(ph)FeP exhibit one of the lowest reactivities even though the value of $\Delta\eta_{DA}$ is the lowest. However, as explained before FePs at the potential at which electrical currents were measured the FePs are predominantly in the inactive state Fe(III)OH. If we compare the activities as *TOF* values which is the activity per active sites (see Fig. 14, Fe porphyrins exhibit the higher *TOF* values. So the activity per active site is higher for complexes exhibiting low $\Delta\eta_{DA}$ values, as expected from the Principle of Lowest Hardness. Finally there is a direct correlation between Fe(III)/(II) redox potential and the energy of the SOMO orbital of FeN4 and also versus the $\Delta\eta_{DA}$ values as illustrated in Fig. S6.

We can propose two possible simple reaction schemes for the catalyst dependence of the rate of TGA oxidation assuming the following mechanism, in which RSH represents TGA, to explicitly show the reactivity of the sulfur atom in TGA. This scheme assumes that the Fe(II) is active, not Fe(III) based on the experimental evidence that at potentials where Fe(III) predominates the activity decrease dramatically as illustrated in Figs. 4 and 8. We can propose two reactions mechanisms; the first involves the non-concerted bond formation and electron transfer, where ET occurs in a rate determining step occurring after bond formation between the Fe center and the sulfur atom:

Since experiments were conducted at pH 13, this value is above the pK= 9.3 of the -SH group in TGA, so all molecules are deprotonated: $HSCH_2CO_2H_{(aq)} + OH^- \leftrightarrows HSCH_2CO_2^-{}_{(aq)} + H_2O$ (pK =3.83) and $HSCH_2CO_2^-{}_{(aq)} + OH^- \leftrightarrows SCH_2CO_2^{=}{}_{(aq)} + H_2O$ pK= 9.3 .

For simplicity we will label $SCH_2CO_2^{=}{}_{(aq)}$ simply as $RS^{=}{}_{(aq)}$

Mechanism I: Non-concerted stepwise ET

$RSH^-{}_{(aq)} + OH^-{}_{(aq)} \leftrightarrows RS^{=}{}_{(aq)} + H_2O$		(i)
$[Fe(I)N_4]^-{}_{ads} \leftrightarrows [Fe(II)N_4]_{ads} + e$		(ii)
$RS^{=}{}_{(aq)} + [Fe(II)N_4]_{ads} \leftrightarrows [Fe(I)N_4\text{-}RS]^{=}{}_{ads}$	bond formation	(iii)
$[Fe(I)N_4\text{-}RS]^{=}{}_{ads} \rightarrow [Fe(II)N_4]_{ads} + RS^{-\cdot}{}_{(aq)} + e^-$	*rds*	(iv)
$2\ RS^{-\cdot}{}_{(aq)} \rightarrow RSSR^{=}{}_{(aq)}$		(v)

where $RSSR^{=}{}_{(aq)} = {}^-CO_2CH_2S\text{-}SCH_2CO_2^-$

Mechanims II : Concerted ET and bond forming mechanism

$RSH^-{}_{(aq)} + OH^-{}_{(aq)} \leftrightarrows$	$RS^{=}{}_{(aq)} + H_2O$	(i)
$[Fe(I)N_4]^-{}_{ads} \leftrightarrows [Fe(II)N_4]_{ads}$	$+ e$	(ii)
$RS^{=}{}_{(aq)} + [Fe(II)N_4]_{ads} \leftrightarrows [Fe(II)N_4\text{-}RS^-]_{ads} + e^-$	*rds*	(vi)
$[Fe(II)N_4\text{-}RS^-]_{ads} \leftrightarrows [Fe(II)N_4]_{ads}$	$+ RS^{-\cdot}{}_{(aq)}$	(v)
$2\ RS^{-\cdot}{}_{(aq)} \rightarrow$	$RSSR^{=}{}_{(aq)}$	(vi)

Finally, Fig. 15 illustrates in a qualitative way the difference between the two possible mechanisms for TGA electroxidation. The

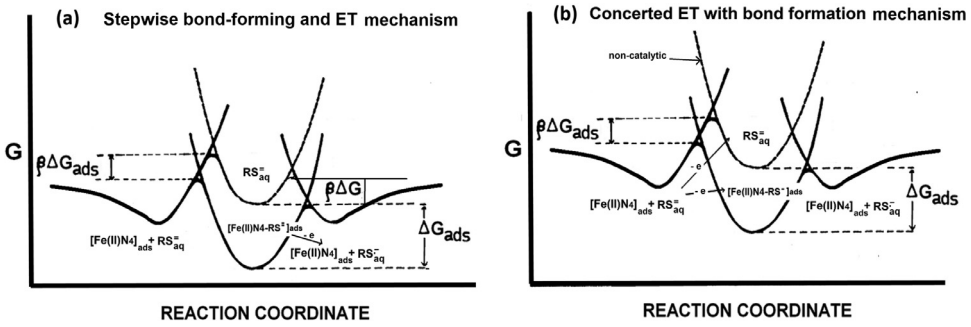

Fig. 15. Comparative qualitative diagram of the two possible mechanisms of ET discussed, (a) stepwise bond formation and then ET (b) concerted bond forming and ET. The free energies are arbitrary and used only for illustration purposes.

equations proposed for the mechanisms explained better the stepwise ET mechanism versus the concerted ET bond formation mechanism as the latter does not explain one of the slopes of the volcano correlations. The Tafel slopes predicted for both mechanisms seem to agree with the experimental data. However, for discriminating between these two mechanims it is necessary to collect more data points investigating a greater number of complexes in order to have more accurate estimation of the Brönsted slopes from volcano correlations especially on the side of the correlation of the Fe porphyrins that exhibit currents in the potential region of OER. It is likely that the mechanism of this process is more complex than described here. We have provided are rather simplistic view of the possible reaction pathways for the reaction and further studies are necessary to have a more complete view of the reaction, especially to have more complete volcano correlations.

4. Conclusions

The purpose of this work was to map several reactivity descriptors for macrocyclic FeN4 complexes for the electrooxidation of TGA. We have studied a series of FeN4 macrocyclic complexes immobilized on pyrolytic graphite and on the outer walls of multiwalled carbon nanotubes, MWCNTs. We examined 4 reactivity descriptors namely the Fe-TGA binding energy, the Fe(III)/(II) formal potential of the complexes, the turn over frequency (*TOF*) and the donor-acceptor intermolecular hardness: Experimental plots of activity as $(\log j)_E$ at constant potential versus the Fe-TGA binding energy and the Fe(III)/(II) redox potential give volcano correlations for both the complexes anchored on OPG or on the external walls of MWCNTs. The activity as $(\log j)_E$ increases with the intermolecular hardness but the *TOFs* exhibit the opposite trends, i.e. decrease with $\Delta\eta_{DA}$ as expected from the Principle of Minimum Hardness. We find linear correlations between the binding energies and the Fe(III)/(II) redox potentials. The redox potentials correlate linearly with the intermolecular hardness and with the energy of the frontier orbitals of the FeN4 complexes indicating that all reactivity descriptors are related to each other. Fe porphyrins exhibit very low activity and require high overpotentials for the reaction to proceed. It is possible that the OER reaction occurs via a parallel pathway on Fe porphyrins. This an issue that needs to be clarified in future work. To avoid OER Fe porphyrins with more positive redox potentials need to be tested and fill the gap in the volcano and other correlations between porphyrins and phthalocyanines.

DFT calculations were carried out in order to understand the role of substituents in the catalytic activity of Fe phthalocyanines and porphyrins, finding that there are two stable conformations of the TGA molecule where oxidation is favored, called “standing” and “lying”, between this molecule and COO^- groups, respectively.

A semi-theoretical plot of catalytic activities $(\log j)_E$ vs DFT calculated TGA binding energies (E_{bTGA}), are consistent with the experimental volcano-type correlations, where in the strong binding side are the electron-acceptor substituents and in the weak side the electron-donors. On the other hand, the Hirshfeld population analysis shows a positive charge on the Fe center of the FeN4 complex, indicating that the electron transfer occurs from TGA to the phthalocyanine or porphyrin complexes, which act as the electron acceptors.

We have proposed two possible mechanisms for the oxidation of TGA: (i) a stepwise and then electron transfer where Fe-S bond formation and the rate determining ET step occur in two different consecutive steps and (ii) a concerted mechanism where Fe-S bond formation and rate determining ET occur in the same step.

Author statement-1

The contributions of the authors are as follows:
Ricardo A. Matute: Conceptualization, Software
Alejandro Toro-Labbé: Conceptualization, Software
María P. Oyarzún: Formal Analysis, Investigation
Sara Ramirez: Formal Analysis, Investigation
Daniela E. Ortega: Conceptualization, Software, Investigation, Methodology, Original draft preparation.
Karina Oyarce: Investigation, Methodology
Nataly Silva: Supervision, Investigation, Conceptualization, Methodology, Project administration, Original draft preparation,Funding acquisition,Writing-Reviewing and Editing.
José H. Zagal: Supervision, Conceptualization, Validation, Project administration, Funding acquisition, Writing-Reviewing and Editing.

Declaration of Competing Interest

The authors declare that they have no known competing financial interests or personal relationships that could have appeared to influence the work reported in this paper.

Acknowledgements

The authors want to ackowledge the funding of Fondecyt Grants 1140199, 1181260 and 1181037, Nucleo Milenio RC 120001 and Conicyt/Anid PIA Project ACT 192175, Dicyt/Usach, Fondecyt Postdoctoral Project 3150271 (N.S) and Conicyt Doctoral Fellowship M.P.O. 21130168. This work partially supported by the NLHPC(ECM-02) supercomputing infrastructure & ANID +REC Convocatoria Nacional Instalacin en la Academia Convocatoria 2020 + PAI77200068.

Supplementary materials

Supplementary material associated with this article can be found, in the online version, at doi:10.1016/j.electacta.2021.138905.

References

[1] M. Tsuda, W.A. Diño, H. Nakanishi, H. Kasai, Orientation dependence of O2 dissociation from heme-O2 adduct, Chem. Phys. Lett. 402 (2005) 71–74, doi:10.1016/j.cplett.2004.12.013.

[2] J. Zagal, M.A. Páez, Electro-oxidation of hydrazine on electrodes modified with vitamin B12, Electrochim. Acta. 42 (1997) 3477–3481, doi:10.1016/S0013-4686(97)00020-0.

[3] G. Ochoa, C. Gutierrez, I. Ponce, J. Francisco Silva, M. Páez, J. Pavez, J.H. Zagal, Reactivity trends of surface-confined Co-tetraphenyl porphyrins and vitamin B12 for the oxidation of 2-aminoethanethiol: comparison with Co-phthalocyanines and oxidation of other thiols, J. Electroanal. Chem. 639 (2010) 88–94, doi:10.1016/j.jelechem.2009.11.027.

[4] K.P. Bryliakov, E.P. Talsi, Active sites and mechanisms of bioinspired oxidation with H 2 O 2 , catalyzed by non-heme Fe and related Mn complexes, Coord. Chem. Rev. 276 (2014) 73–96, doi:10.1016/j.ccr.2014.06.009.

[5] A.B. Sorokin, Phthalocyanine metal complexes in catalysis, Chem. Rev. 113 (2013) 8152–8191, doi:10.1021/cr4000072.

[6] J.H. Zagal, S. Griveau, J.F. Silva, T. Nyokong, F. Bedioui, Metallophthalocyanine-based molecular materials as catalysts for electrochemical reactions, Coord. Chem. Rev. 254 (2010) 2755–2791, doi:10.1016/j.ccr.2010.05.001.

[7] G.I. Cárdenas-Jirón, M.A. Gulppi, C.A. Caro, R. del Río, M. Páez, J.H. Zagal, Reactivity of electrodes modified with substituted metallophthalocyanines. Correlations with redox potentials, Hammett parameters and donor-acceptor intermolecular hardness, Electrochim. Acta. 46 (2001) 3227–3235, doi:10.1016/S0013-4686(01)00614-4.

[8] J.H. Zagal, M.T.M. Koper, Reactivity descriptors for the activity of molecular MN4 catalysts for the oxygen reduction reaction, Angew. Chemie. 55 (2016) 14510–14521, doi:10.1002/anie.201604311.

[9] J. Masa, W. Schuhmann, Systematic selection of metalloporphyrin-based catalysts for oxygen reduction by modulation of the donor-acceptor intermolecular hardness, Chem. - A Eur. J. 19 (2013) 9644–9654, doi:10.1002/chem.201203846.

[10] J. Masa, K. Ozoemena, W. Schuhmann, J.H. Zagal, Oxygen reduction reaction using N4-metallomacrocyclic catalysts: fundamentals on rational catalyst design, J. Porphyr. Phthalocyanines. 16 (2012) 761–784, doi:10.1142/S1088424612300091.

[11] N. Ramaswamy, U. Tylus, Q. Jia, S. Mukerjee, Activity descriptor identification for oxygen reduction on nonprecious electrocatalysts: linking surface science to coordination chemistry, J. Am. Chem. Soc. 135 (2013) 15443–15449, doi:10.1021/ja405149m.

[12] J.H. Zagal, G.I. Cárdenas-Jirón, Reactivity of immobilized cobalt phthalocyanines for the electroreduction of molecular oxygen in terms of molecular hardness, J. Electroanal. Chem. 489 (2000) 96–100, doi:10.1016/S0022-0728(00)00209-6.

[13] J. Masa, K. Ozoemena, W. Schuhmann, J.H. Zagal, Oxygen reduction reaction using N 4 -metallomacrocyclic catalysts: fundamentals on rational catalyst design, J. Porphyr. Phthalocyanines. 16 (2012) 761–784, doi:10.1142/S1088424612300091.

[14] J.H. Zagal, P. Herrera, Electrochemistry of cysteine and cystine on metal-phthalocyanines adsorbed on a graphite electrode, Electrochim. Acta. 30 (1985) 449–454, doi:10.1016/0013-4686(85)80033-5.

[15] C.A. Gutierrez, J.F. Silva, F.J. Recio, S. Griveau, F. Bedioui, C.A. Caro, J.H. Zagal, In search of the best iron N4-macrocyclic catalysts adsorbed on graphite electrodes and on multi-walled carbon nanotubes for the oxidation of l-cysteine by adjusting the Fe(II)/(I) formal potential of the complex, Electrocatalysis 5 (2014) 426–437, doi:10.1007/s12678-014-0209-y.

[16] M.J. Aguirre, M. Isaacs, F. Armijo, L. Basáez, J.H. Zagal, Effect of the substituents on the ligand of iron phthalocyanines adsorbed on graphite electrodes on their activity for the electrooxidation of 2-mercaptoethanol, Electroanalysis 14 (2002) 356–362, doi:10.1002/1521-4109(200203)14:5⟨356::AID-ELAN356⟩3.0.CO;2-U.

[17] C. Gutiérrez-Cerón, M.A. Páez, J.H. Zagal, Reactivity descriptors for iron porphyrins and iron phthalocyanines as catalysts for the electrooxidation of reduced glutathione, J. Solid State Electrochem. 20 (2016) 3199–3208, doi:10.1007/s10008-016-3396-z.

[18] C. Gutiérrez-Cerón, N. Silva, I. Ponce, J.H. Zagal, Testing reactivity descriptors for the electrocatalytic activity of OPG hybrid electrodes modified with iron macrocyclic complexes and MWCNTs for the oxidation of reduced glutathione in basic medium, Russ. J. Electrochem. 55 (2019) 1136–1143, doi:10.1134/S1023193519110077.

[19] F.J. Recio, P. Cañete, F. Tasca, C. Linares-Flores, J.H. Zagal, Tuning the Fe(II)/(I) formal potential of the FeN4 catalysts adsorbed on graphite electrodes to the reversible potential of the reaction for maximum activity: hydrazine oxidation, Electrochem. Commun. 30 (2013) 34–37, doi:10.1016/j.elecom.2013.01.024.

[20] F. Tasca, F.J. Recio, R. Venegas, D. a. Geraldo, M. Sancy, J.H. Zagal, Linear versus volcano correlations for the electrocatalytic oxidation of hydrazine on graphite electrodes modified with MN4 macrocyclic complexes, Electrochim. Acta. 140 (2014) 314–319, doi:10.1016/j.electacta.2014.04.059.

[21] J.H. Zagal, F. Bedioui, J.-P. Dodelet, N4-Macrocyclic Metal Complexes, Springer, New York, 2006, doi:10.1007/978-0-387-28430-9.

[22] P. Castro-Latorre, S. Miranda-Rojas, L. Barrientos, F. Mendizabal, Catalytic activity of iron phthalocyanine for the oxidation of thiocyanate and L-cysteine anchored on Au(111) clusters, Mol. Simul. 45 (2019) 1447–1453, doi:10.1080/08927022.2019.1654607.

[23] E.M. Bruti, M. Giannetto, G. Mori, R. Seeber, Electropolymerization of tetrakis(o-aminophenyl)porphyrin and relevant transition metal complexes from aqueous solution. The resulting modified electrodes as potentiometric sensors, Electroanalysis 11 (1999) 565–572, doi:10.1002/(SICI)1521-4109(199906)11:8⟨565::AID-ELAN565⟩3.0.CO;2-V.

[24] N. Silva, C. Castro-Castillo, M.P. Oyarzún, S. Ramírez, C. Gutierrez-Ceron, J.F. Marco, J.F. Silva, J.H. Zagal, Modulation of the electrocatalytic activity of Fe phthalocyanine to carbon nanotubes: electrochemistry of l-cysteine and l-cystine, Electrochim. Acta. 308 (2019) 295–306, doi:10.1016/j.electacta.2019.04.005.

[25] N. Silva, S. Calderón, M.A. Páez, M.P. Oyarzún, M.T.M. Koper, J.H. Zagal, Probing the Fen+/Fe(n−1)+ redox potential of Fe phthalocyanines and Fe porphyrins as a reactivity descriptor in the electrochemical oxidation of cysteamine, J. Electroanal. Chem. 819 (2018) 502–510, doi:10.1016/j.jelechem.2017.12.068.

[26] F.J. Recio, C.A. Gutierrez, J.F. Silva, F.J. Recio, S. Griveau, In search of the best iron N-4-macrocyclic catalysts adsorbed on graphite electrodes and on multi-walled carbon nanotubes for the oxidation of L-cysteine by adjusting the Fe(II)/(I) formal potential of the complex, Electrocatalysis 5 (2014) 426–437, doi:10.1007/s12678-014-0209-y.

[27] P. Avouris, Z. Chen, V. Perebeinos, Carbon-based electronics, Nat. Nanotechnol. 2 (2007) 605–615, doi:10.1038/nnano.2007.300.

[28] S. Berber, Y. Kwon, D. Tománek, Unusually high thermal conductivity of carbon nanotubes, Phys. Rev. Lett. 84 (2000) 4613–4616.

[29] R. Venegas, F.J. Recio, J. Riquelme, H. Zagal, Biomimetic reduction of O2 in an acid medium on iron phthalocyanines axially coordinated to pyridine anchored on carbon nanotubes, J. Mater. Chem. A. 5 (2017) 12054–12059, doi:10.1039/c7ta02381b.

[30] A. Morozan, S. Campidelli, A. Filoramo, B. Jousselme, S. Palacin, Catalytic activity of cobalt and iron phthalocyanines or porphyrins supported on different carbon nanotubes towards oxygen reduction reaction, Carbon N. Y. 49 (2011) 4839–4847, doi:10.1016/j.carbon.2011.07.004.

[31] J.H. Zagal, S. Griveau, M. Santander-Nelli, S.G. Granados, F. Bedioui, Carbon nanotubes and metalloporphyrins and metallophthalocyanines-based materials for electroanalysis, J. Porphyr. Phthalocyanines. 16 (2012) 713–740, doi:10.1142/S1088424612300054.

[32] R. Rippel, Mercaptoacetic acid and derivatives, Ullmann's Encycl. Ind. Chem. (2012) 30–33, doi:10.1002/14356007.a16.

[33] S. Shahrokhian, J. Yazdani, Electrocatalytic oxidation of thioglycolic acid at carbon paste electrode modified with cobalt phthalocyanine : application as a potentiometric sensor, Electrochim. Acta. 48 (2003) 4143–4148, doi:10.1016/S0013-4686(03)00582-6.

[34] L.-H. Wang, Z.-S. Chen, Determination of thioglycolic acid and cysteine in hair-treatment products at ceramic carbon composite electrodes, Electroanalysis 9 (1997) 1294–1297, doi:10.1002/elan.1140091616.

[35] J. Sun, D.M. Stanbury, Kinetics and mechanism of oxidation of thioglycolic acid by hexachloroiridate, J. Chem. Soc. Dalt. Trans. (2002) 785–791, doi:10.1039/b105951n.

[36] S. Gangopadhyay, M. Ali, A. Dutta, P. Banerjee, Oxidation of thioglycolic acid and glutathione by (trans - cyclohexane-1,2-diamine - N,N,N ',N '-tetraacetato) manganate(iii) in aqueous media, J. Chem. Soc. Dalt. Trans. (1994) 841–845, doi:10.1039/DT9940000841.

[37] G.A. Ayoko, M.A. Olatljnji, Oxidation of L-cysteine, mercaptoacetic acid and b-mercaptoethylamine by 12-tungstocobaltate(III), Polyhedron 2 (1983) 577–582, doi:10.1016/S0277-5387(00)81513-2.

[38] R.C. Kapoor, O.P. Kachhwaha, B.P. Sinha, Oxidation kinetics of thioglycolic acid by ferricyanide ion in acid medium, J. Phys. Chem. 73 (1969) 1627–1631, doi:10.1021/j100726a001.

[39] F. Neese, Software update: the ORCA program system, version 4.0, Wires Comput. Mol. Sci. 8 (2018) 1–6, doi:10.1002/wcms.1327.

[40] J.P. Perdew, K. Burke, M. Ernzerhof, Generalized gradient approximation made simple, Phys. Rev. Lett. 77 (1996) 3865–3868, doi:10.1103/PhysRevLett.77.3865.

[41] M. Dolg, U. Wedig, H. Stoll, H. Preuss, W. Germany, Energy adjusted ab initio pseudopotentials for the first row transition elements, J. Chem. Phys. 86 (1987) 866–872, doi:10.1063/1.452288.

[42] F. Weigend, R. Ahlrichs, Balanced basis sets of split valence, triple zeta valence and quadruple zeta valence quality for H to Rn: design and assessment of accuracy, Phys. Chem. Chem. Phys. 7 (2005) 3297–3305, doi:10.1039/b508541a.

[43] M.L. Pegis, B.A. McKeown, N. Kumar, K. Lang, D.J. Wasylenko, X.P. Zhang, S. Raugei, J.M. Mayer, Homogenous electrocatalytic oxygen reduction rates correlate with reaction overpotential in acidic organic solutions, ACS Cent. Sci. 2 (2016) 850–856, doi:10.1021/acscentsci.6b00261.

[44] S. Grimme, J. Antony, S. Ehrlich, H. Krieg, S. Grimme, J. Antony, S. Ehrlich, H. Krieg, A consistent and accurate ab initio parametrization of density functional dispersion correction (DFT-D) for the 94 elements H-Pu, J. Chem. Phys. 132 (2010) 154104, doi:10.1063/1.3382344.

[45] S.F. Boys, F. Bernardi, The calculation of small molecular interactions by the differences of separate total energies. Some procedures with reduced errors, Mol. Phys. 19 (1970) 553–566, doi:10.1080/00268977000101561.

[46] Y. Takano, K.N. Houk, L. Angeles, L. Angeles, Benchmarking the Conductor-like Polarizable Continuum Model (CPCM) for Aqueous Solvation Free Energies of Neutral and Ionic Organic Molecules, J. Chem. Theory Comput. 1 (2005) 70–77, doi:10.1021/ct049977a.

[47] E.R. Davidson, S. Chakravorty, A test of the Hirshfeld definition of atomic charges and moments, Theor. Chim. Acta. 83 (1992) 319–330, doi:10.1007/BF01113058.

[48] C.F. Matta, R.J. Boyd, An Introduction to the Quantum Theory of Atoms in Molecules, in: Quantum Theory Atoms Mol, Wiley-VCH Verlag GmbH & Co. KGaA, Weinheim, Germany, 2007, pp. 1–34, doi:10.1002/9783527610709.ch1.

[49] D. Qi, X. Chen, W. Liu, C. Liu, W. Liu, K. Wang, J. Jiang, A Ni/Fe-based heterometallic phthalocyanine conjugated polymer for the oxygen evolution reaction, Inorg. Chem. Front. 7 (2020) 642–646, doi:10.1039/c9qi01325c.
[50] N. Uwitonze, D. Zhou, J. Lei, W. Chen, X.Q. Zuo, J. Cai, Y.X. Chen, The high Tafel slope and small potential dependence of activation energy for formic acid oxidation on a Pd electrode, Electrochim. Acta. 283 (2018) 1213–1222, doi:10.1016/j.electacta.2018.07.074.
[51] A. Morozan, S. Campidelli, A. Filoramo, B. Jousselme, S. Palacin, Catalytic activity of cobalt and iron phthalocyanines or porphyrins supported on different carbon nanotubes towards oxygen reduction reaction, Carbon N. Y. 49 (2011) 4839–4847, doi:10.1016/j.carbon.2011.07.004.
[52] H.A. Gasteiger, S.S. Kocha, B. Sompalli, F.T. Wagner, Activity benchmarks and requirements for Pt, Pt-alloy, and non-Pt oxygen reduction catalysts for PEMFCs, Appl. Catal. B Environ. 56 (2005) 9–35, doi:10.1016/j.apcatb.2004.06.021.
[53] M. Lopez-Tenes, J. Gonzalez, A. Molina, Two-electron transfer reactions in electrochemistry for solution-soluble and surface-confined molecules: A common approach, J. Phys. Chem. C. 118 (2014) 12312–12324, doi:10.1021/jp5025763.
[54] B. Limoges, J.M. Savéant, Catalysis by immobilized redox enzymes. Diagnosis of inactivation and reactivation effects through odd cyclic voltammetric responses, J. Electroanal. Chem. 562 (2004) 43–52, doi:10.1016/j.jelechem.2003.07.035.
[55] G.I. Cárdenas-Jirón, J.H. Zagal, Donor–acceptor intermolecular hardness on charge transfer reactions of substituted cobalt phthalocyanines, J. Electroanal. Chem. 497 (2001) 55–60, doi:10.1016/S0022-0728(00)00434-4.